

The landscape of biomedical research

Rita González-Márquez^{1,2}, Luca Schmidt^{1,2}, Benjamin M. Schmidt³,
Philipp Berens^{1,2,4}, and Dmitry Kobak^{1,2}

¹*Hertie Institute for AI in Brain Health, University of Tübingen, Germany*

²*Institute for Ophthalmic Research, University of Tübingen, Germany*

³*Nomic AI, New York, USA*

⁴*Tübingen AI Center, Tübingen, Germany*

✉ dmitry.kobak@uni-tuebingen.de

May 25, 2023

Abstract

The number of publications in biomedicine and life sciences has rapidly grown over the last decades, with over 1.5 million papers now being published every year. This makes it difficult to keep track of new scientific works and to have an overview of the evolution of the field as a whole. Here we present a 2D map of the entire corpus of biomedical literature, and argue that it provides a unique and useful overview of the life sciences research. We based our atlas on the abstract texts of 21 million English articles from the PubMed database. To embed the abstracts into 2D, we used the large language model PubMedBERT, combined with t-SNE tailored to handle samples of our size. We used our atlas to study the emergence of the Covid-19 literature, the evolution of the neuroscience discipline, the uptake of machine learning, the distribution of gender imbalance in academic authorship, and the distribution of retracted paper mill articles. Furthermore, we present an interactive web version of our atlas that allows easy exploration and will enable further insights and facilitate future research.

1 Introduction

The rate of scientific publishing has been increasing constantly over the past century (Larsen and von Ins, 2010; Bornmann and Mutz, 2015), with over one million articles being currently published every year in biomedicine and life sciences alone. Information about academic publications in these fields is collected in the PubMed database, maintained by the United States National Library of Medicine (pubmed.ncbi.nlm.nih.gov). It now contains over 33 million scientific papers from the last 50 years.

This rapid growth of the biomedical literature makes it difficult to track the evolution of biomedical publishing as a whole. Search engines like PubMed and Google Scholar allow researchers to find specific papers given suitable keywords and to follow the citation networks that these papers are embedded in, yet none of them allows exploration of the biomedical literature ‘landscape’ from a global perspective. This makes it hard to see how research topics evolve over time, how different fields are related to each other, or how new methods and techniques are adopted in different fields. What is needed to answer such questions, is a bird’s-eye view on the biomedical literature.

In this work we develop an approach that enables all of the above: a global two-dimensional atlas of the biomedical and life science literature which is based on the ab-

stracts of all 21 million English language articles contained in the PubMed database. To create the map, we embedded the abstracts into two dimensions using the transformer-based large language model PubMedBERT (Gu et al., 2021) combined with the neighbor embedding method t-SNE (van der Maaten and Hinton, 2008). Adapting this pipeline to handle sample sizes on the scale of this entire corpus of biomedical literature, our approach allowed us to create a map with the level of detail exceeding previous work by three orders of magnitude (Boyack et al., 2020; Börner et al., 2012).

We argue that our visualization facilitates exploration of the biomedical literature and can reveal aspects of the data that would not be easily noticed with other analysis methods. We showcase the power of our approach in five examples: we studied (1) the emergence of the Covid-19 literature, (2) the evolution of different subfields of neuroscience, (3) the uptake of machine learning in the life sciences, (4) the distribution of gender imbalance across biomedical fields, and (5) the distribution of retracted paper mill articles. In all cases, we used the embedding to formulate specific hypotheses about the data that were later confirmed by a dedicated statistical analysis of the original high-dimensional dataset.

The resulting map of the biomedical research landscape is publicly available as an interactive web version at <https://static.nomic.ai/pubmed.html>, developed us-

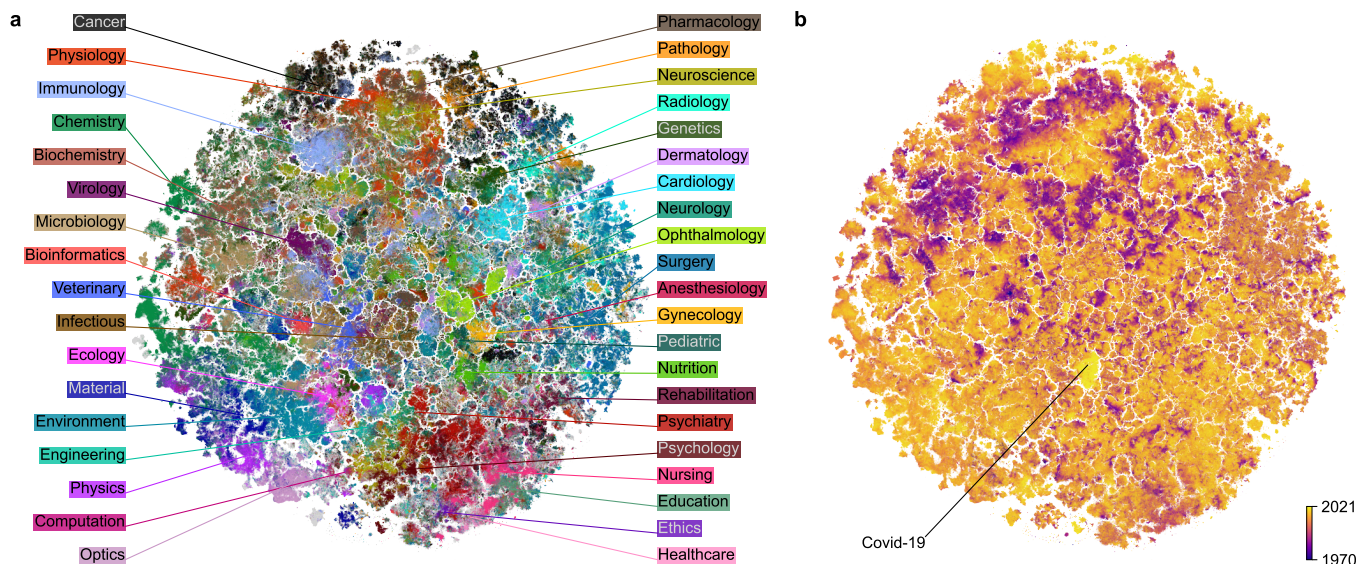


Figure 1: 2D embedding of the PubMed dataset. Paper abstracts ($n = 21\text{ M}$) were transformed into 768-dimensional vectors with PubMedBERT (Gu et al., 2021) and then embedded in 2D with t -SNE (van der Maaten and Hinton, 2008). (a) Coloured using labels based on journal titles. Unlabeled papers are shown in gray and are displayed in the background. (b) Coloured by publication year (dark: 1970 and earlier; light: 2021).

Table 1: Quality metrics for the embeddings. Acc.: k NN accuracy ($k = 10$) of label prediction. RMSE: root-mean-squared error of k NN prediction of publication year. Recall: overlap between k nearest neighbours in the 2D embedding and in the high-dimensional space. See Methods for details.

Data	Dim.	Acc.	RMSE	Recall
PubMedBERT	768	69.7%	8.4	—
TF-IDF	4,679,130	65.2%	8.8	—
t -SNE(BERT)	2	62.6%	10.2	6.2%
t -SNE(TF-IDF)	2	50.6%	11.2	0.7%
Chance	—	4.3%	12.4	0.0%

ing the deepscatter library (Nomic AI, 2022). It allows users to navigate the atlas, zoom, and search by article title and journal name, while loading individual scatter points on demand. We envisage that the interactive embedding will allow further insights into the biomedical literature, beyond the ones we present in this work.

2 Results

2.1 Two-dimensional atlas allows to explore the PubMed database

We downloaded the complete PubMed database and, after initial filtering (see Methods), were left with 20,687,150 papers with valid English abstracts, the majority of which (99.8%) were published in 1970–2021 (Figure S1). Our goal was to generate a 2D embedding of the abstract texts to facilitate exploration of the data. All

our embeddings were based on the abstract texts alone, and did not use any further metadata or information on citations or references.

To annotate our atlas, we chose a set of 38 labels covering basic life science fields such as ‘virology’ and ‘biochemistry’, and medical specialties such as ‘radiology’ and ‘ophthalmology’. We assigned each label to the papers published in journals with the corresponding word in journal titles. For example, all papers published in *Annals of Surgery* were labeled ‘surgery’. As a result, 34.4% of all papers received a label, while the rest remained unlabeled.

To generate a two-dimensional map of the entire PubMed database, we first obtained a 768-dimensional numerical representation of each abstract using PubMedBERT (Gu et al., 2021), which is a Transformer-based (Vaswani et al., 2017) language model trained on PubMed abstracts and full-text articles from PubMed Central. We then reduced the dimensionality to two using t -SNE (van der Maaten and Hinton, 2008).

For the initial step of computing a numerical representation of the abstracts, we evaluated several text processing methods, including bag-of-words representations such as TF-IDF (Jones, 1972) and several other BERT-derived models, including the original BERT (Devlin et al., 2019), SBERT (Reimers and Gurevych, 2019), SciBERT (Beltagy et al., 2019), BioBERT (Lee et al., 2020), SPECTER (Cohan et al., 2020), SimCSE (Gao et al., 2021), and SciNCL (Ostendorff et al., 2022). We chose PubMedBERT because it best grouped papers together in terms of their label, quantified by the k -nearest-neighbour (k NN) classification accuracy when each label is predicted based on the most frequent label of its 10 nearest neighbors (Table 3). For the PubMedBERT representation, this

prediction was correct 69.7% of the time (Table 1). For comparison, TF-IDF, which is simpler and faster to compute, yielded lower k NN accuracy (65.2%).

For the second step, we used t -SNE with several modifications that allowed us to run it effectively on very large datasets. These modifications included uniform affinities to reduce memory consumption and extended optimization to ensure better convergence (see Methods). With these modifications, t -SNE performs better than other neighbour embedding methods such as UMAP (McInnes et al., 2018) in terms of k NN accuracy and memory requirements (González-Márquez et al., 2022). The resulting embedding showed good label separation, with k NN accuracy in 2D of 62.6%, not much worse than in the 4,679,130-dimensional TF-IDF representation.

We interpret the resulting embedding as the map of the biomedical literature (Figure 1). It showed sensible global organization, with natural sciences mainly located on the left side and medical specialties gathered on the right side; physics- and engineering-related works occupied the bottom-left part (Figures S2, S3). Related disciplines were located next to each other: for example, the biochemistry region was overlapping with chemistry, whereas psychology was merging into psychiatry. A t -SNE embedding based on the TF-IDF representation had similar large-scale structure but worse k NN accuracy (50.6%; Figure S4).

In addition to this global structure, the map revealed rich and detailed fine structure and was fragmented into small clusters containing hundreds to thousands of papers each (Figure S5a). Even though immediate neighborhoods were distorted compared to the 768-dimensional PubMedBERT representation (only 6.2% of the nearest neighbors in \mathbb{R}^2 were nearest neighbors in \mathbb{R}^{768} ; we call this metric k NN recall), manual inspection of the clusters suggested that they consisted of papers on clearly-defined narrow topics.

Moreover, the map had rich temporal structure, with papers of the same age tending to be grouped together (Figure 1b). While this structure may be influenced by changes in writing style and common vocabulary, it is likely primarily caused by research topics evolving over time and becoming more or less fashionable. The most striking example of this effect is a cluster of very recent papers published in 2020–21 that is very visible in the middle of the map (bright yellow in Figure 1b). We will use this island as our first example of how the map can be used to guide understanding of the publishing landscape and how it allows to form hypotheses about the structure and temporal evolution of biomedical research. We will show that these hypotheses can be rigorously confirmed in the high-dimensional embedding space.

2.2 The Covid-19 literature is uniquely isolated

The bright yellow island we identified above comprised works related to Covid-19 (Figure 1b). Our dataset

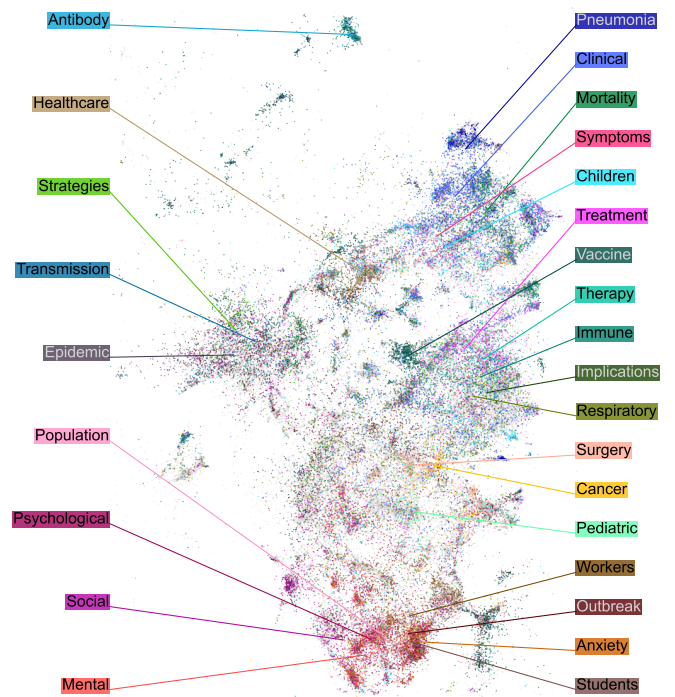


Figure 2: Covid-19 region of the map. Colours are assigned using labels based on paper titles. Unlabeled Covid papers are shown in the background in gray. This region in the embedding also contained some non-Covid papers (~15%) about other respiratory epidemics; they are not shown.

included 132,802 Covid-related papers (based on terms such as COVID-19, SARS-CoV-2, etc., present in their abstracts; see Methods), which constituted 5.2% of all PubMed papers published in 2020–2022. As the pandemic and its effects were studied by many different biomedical fields, one might have expected the Covid papers to be distributed across the embedding in their corresponding disciplines. Instead, we found that 59.3% out of all Covid-related papers were grouped together in one cluster (Figure 1b), while the rest were sparsely distributed across the map (Figure S6a).

The main Covid cluster was surrounded by articles on other epidemics, public health issues, and respiratory diseases. When we zoomed in, we found rich inner structure within the Covid cluster itself, with multiple Covid-related topics separated from each other (Figure 2). Papers on mental health and societal impact, on public health and epidemiological control, on immunology and vaccines, on clinical symptoms and treatment — were all largely non-overlapping, and were further divided into even narrower subfields. This suggests that our map can be useful for navigating the literature on the scale of narrow and focused scientific topics.

Seeing that the Covid papers prominently stood out in the map (Figure 1b), we hypothesized that the Covid literature was more isolated from the rest of the biomedical literature, compared to other similar fields. To test this, we selected several comparable sets of papers, such as pa-

Table 2: Isolatedness metric for several sets of papers.

Fraction of k -nearest-neighbors of papers from each corpus that also belong to the same corpus (see Methods). The first four rows show corpora selected based on the abstract text; the last two — based on the journal name.

	n	BERT	TF-IDF
Covid-19	132,802	80.6%	76.2%
HIV/AIDS	308,077	63.9%	62.3%
Influenza	90,575	57.9%	64.1%
Meta-analysis	145,358	52.6%	38.5%
Virology	112,807	47.7%	39.1%
Ophthalmology	144,411	47.7%	43.6%

pers on HIV/AIDS or influenza, or all papers published in virology or ophthalmology journals (two labels that appeared particularly compact in Figure 1a). We measured the *isolatedness* of each corpus in the high-dimensional space by the fraction of their k NNs that belonged to the same corpus. We found that indeed, Covid literature had the highest isolatedness, in both BERT (80.6%) and TF-IDF (76.2%) representations (Table 2). This suggests that the Covid-19 pandemic had an unprecedented effect on the scientific literature, creating a separate and uniquely detached field of study in only two years.

In the TF-IDF version of the embedding (Figure S4b), the Covid cluster appeared even more separated from the rest of the embedding, and included a larger fraction of Covid papers (86.7%), compared to the BERT-based embedding. We observed the same effect with several other paper subsets. For example, in the TF-IDF-based embedding, meta-analysis papers as well as papers on HIV were grouped together and isolated stronger than in the BERT-based embedding (Figure S6b). This suggests that TF-IDF representation is more sensitive to the presence of specific keywords, whereas the BERT representation is more faithful to semantic similarity between fields (e.g. between Covid papers and the literature on other respiratory diseases).

2.3 Changing focus within neuroscience

As we have seen in the extreme example of the Covid literature, the atlas can be used to study composition and temporal trends across disciplines. We next show how it can also provide insights into shifting topics and trends inside a discipline. We demonstrate this using the example of neuroscience. Neuroscience papers ($n = 240,135$) in the map were divided into two main clusters (Figure 3a). The upper one contained papers on molecular and cellular neuroscience, while the lower one consisted of studies on behavioral and cognitive neuroscience. Several smaller clusters comprised papers on neurodegenerative diseases and sensory systems.

Colouring this part of the embedding by publication year indicated that the cellular/molecular region on average had older papers than the cognitive/behavioural re-

gion (Figure 3b). This suggests that the relative publication volume in different subfields of neuroscience has changed with time. To test this hypothesis directly, we devised a metric measuring the overlap between neuroscience and any given related discipline across time. We defined kNN *overlap* as the fraction of k NNs of neuroscience papers that belonged to a given discipline in the high-dimensional space. We found that the overlap of neuroscience with physiology and pharmacology has decreased since the 1970s, while its overlap with psychiatry, psychology, and computation has increased, in particular after 1990s (Figure 3c). Indeed, neuroscience originated as a study of the nervous system within physiology, but gradually broadened its scope to include cognitive neuroscience, related to psychology, as well as computational neuroscience, related to computer science and machine learning.

2.4 The uptake of machine learning

We next used visual exploration of the map to form hypotheses about the uptake of new techniques across different biomedical domains. In recent years, computational methods such as machine learning have increasingly found use in various biomedical disciplines. To explore the use of machine learning (ML), we identified 342,070 papers (1.7%) mentioning some of the most popular ML and statistical methods in their abstracts (Figure 4a). We found that the medical part of the embedding was dominated by classical linear methods such as linear regression and factor analysis, whereas more modern nonlinear and nonparametric methods were mostly used in non-medical research.

Papers claiming to use machine learning ($n = 38,446$ papers containing the phrase ‘machine learning’ in their abstracts) were also rare in the medical part of the PubMed corpus. In the embedding, they were grouped into several clusters, covering topics ranging from computational biology to healthcare data management (Figure 4b). We selected and manually labeled 12 prominent ML-heavy regions of the embedding (Figure 4b), and computed the fraction of papers within each region mentioning specific ML and statistical methods (Table S1). We found that the usage of ML techniques varied strongly across disciplines. Deep learning and convolutional networks were prominent in the image segmentation region (with applications e.g. in microscopy). Clustering was often used in analyzing sequencing data. Neural networks and support vector machines were actively used in structural biology. Principal component analysis was important for data analysis in mass spectrometry. Overall, Figures 4a–b provide a bird’s eye view on the usage of ML across biomedical fields.

Within the medical part of the corpus, ML papers were concentrated in several regions, such as e.g. analysis of tumor imaging. This suggests that different medical disciplines have not been equally quick to adopt ML methods. We confirmed this by computing the fraction of ML pa-

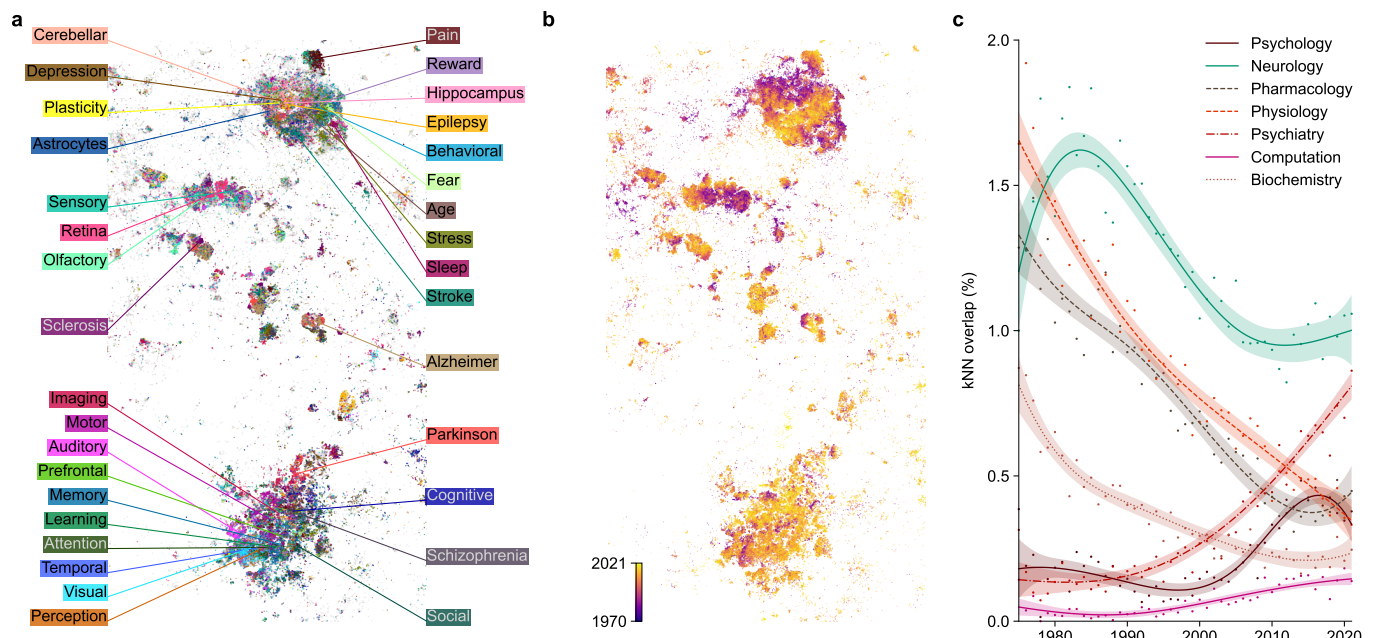


Figure 3: Neuroscience literature. (a) Articles published in neuroscience journals, coloured by presence of specific words in paper titles. (b) The same articles coloured by the publication year (dark: 1970 and earlier; light: 2021). (c) Fraction of the high-dimensional k NNs of neuroscience papers that belonged to a given discipline (biochemistry, computation, neurology, pharmacology, physiology, psychiatry, psychology). Points: yearly averages. Smooth curves and 95% confidence intervals were obtained with generalized additive models (see Methods).

pers within different disciplines across time (Figure 4c). We found that radiology was the first to show increase in ML adoption, shortly after 2015, followed by psychiatry and neurology. In oncology, ML adoption started later but showed accelerated rise over the last five years. This is in contrast with specialties like dermatology and gynecology that did not see any ML usage until \sim 2020.

2.5 Exploring the gender gap

Finally, we will show how the map can be used to explore and better understand social disparities in biomedical publishing such as the extent and distribution of the well-known gender imbalance in academic authorship (Filaro et al., 2016; Larivière et al., 2013; Shen et al., 2018; Dworkin et al., 2020; Bendels et al., 2018). We used the first name (where available) of the first and the last author of every PubMed paper to infer their gender using the `gender` tool (Blevins and Mullen, 2015). The gender inference is only approximate, as some first names may have been absent in the training data and some other names are inherently gender-ambiguous (see Methods). Still, this procedure allowed us to obtain inferred genders for 40.7% of all papers. Among those papers, 42.4% of first authors and 29.1% of last authors were female. While some academic fields, such as mathematics and physics, tend to prefer alphabetic ordering of the authors, in biomedicine the first author is usually the trainee (PhD student or postdoc) who did the practical hands-on project work and the last author is the supervisor or prin-

cipal investigator.

Unsurprisingly, coloring the embedding by gender showed that female authors were not equally distributed across the biomedical publishing landscape (Figure 5a,b). First and last female authors were most frequent in the lower right corner of the embedding, covering topics like nursing, education, and psychology. Only here we found the map to be visually indicative of a large proportion of female senior authors. In contrast, engineering-related disciplines were predominantly male, as well as some medical specialties such as surgery.

There was substantial heterogeneity of gender ratios within some of the individual disciplines, and our fine-grained map allowed us to zoom in further. For example, in healthcare (overall 49.6% female first authors), there were male- and female-dominated regions in the map. One of the more male-dominated clusters (33.9% female) focused on financial management while one of the more female ones (68.1% female) — on patient care (Figure 5c). In education (58.6% female authors), female authors dominated research on nursing training whereas male authors were more frequent in research on medical training (Figure 5d). In surgery, only 24.4% of the first authors were female, but this fraction increased to 61.1% in the cluster of papers on veterinary surgery (Figure 5e). This agrees with veterinary medicine being a predominantly female discipline (52.2% in total, Figure 5g). Importantly, these details may be lost when averaging across a priori labels, while the embedding can suggest the relevant level of granularity.

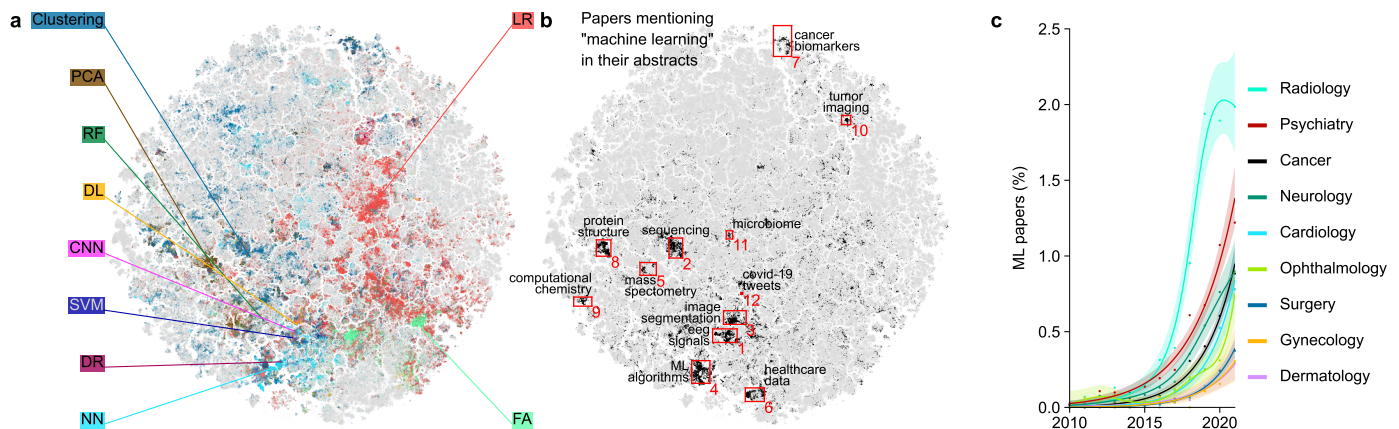


Figure 4: Machine learning papers. (a) Papers coloured according to various statistical and machine learning methods mentioned in their abstracts. Abbreviations: principal component analysis (PCA), random forest (RF), deep learning (DL), convolutional neural network (CNN), support vector machine (SVM), dimensionality reduction (DR), neural networks (NN), linear regression (LR), factor analysis (FA). Some of the highlighted NN papers may refer to biological neural networks. (b) Papers containing ‘machine learning’ phrase in their abstracts, grouped into 12 clusters that we manually labeled. (c) Percentage of papers mentioning ‘machine learning’ in their abstracts across time for different disciplines. Points: yearly percentages. Smooth curves and 95% confidence intervals were obtained using generalized additive models (see Methods).

Analyzing the gender ratios across time, we found that the fraction of female authors steadily increased with time (Figure 5f), with first and last authors being 47.2% and 34.4% female in 2021. We found a delay of ~ 20 years between the first and the last author curves, suggesting that it takes more than one academic generation for the differences in gender bias to propagate from mentees to mentors.

Looking at individual disciplines, we found that the fraction of female first authors increased with time in all of them (Figure 5g), even in disciplines where this fraction was already high, such as education (increased from 55% female in 2005 to 60% in 2020). This increase also happened in male-dominated fields such as computation, physics, or surgery (increase from 15–20% to 25%). Notably, the female proportion in material sciences showed only a modest increase while nursing, the most female-dominated discipline across all our labels (80.4%) even showed a moderate decrease.

2.6 Retracted papers highlight suspicious literature

We identified 11,756 retracted papers with intact abstracts (not containing words like “retracted” or “withdrawn”; see Methods) in our dataset. These papers were not distributed uniformly over the 2D map (Figure 6) but instead concentrated in several specific areas, in particular on top of the map, covering research on cancer-related drugs, marker genes, and microRNA. These areas are known targets of paper mills (Byrne and Labbé, 2017; Byrne et al., 2019; Candal-Pedreira et al., 2022), which are for-profit organizations that produce fraudulent research papers and sell the authorship.

Our map is based solely on textual similarity between

abstracts. This suggests that non-retracted papers from the regions with high concentration of retracted papers may require an investigation, as their abstracts are similar to the ones from paper mill products. We considered a region with particularly high fraction (48/443) of retracted papers (second inset in Figure 6) and randomly selected 25 non-retracted papers for manual inspection. They had similar title format (variations of “MicroRNA-X does Y by targeting Z in osteosarcoma”), paper structure, and figure style, and 24/25 of them had authors affiliated with Chinese hospitals — features that are often shared by paper mill products (Byrne, 2019; Byrne and Christopher, 2020; Else and Van Noorden, 2021; Zhao et al., 2021; Candal-Pedreira et al., 2022). Even though none of this guarantees that these papers are fraudulent, our results suggest that the 2D map can be used to highlight papers requiring further editorial investigation. Moreover, if additional paper mills are discovered in the future, our map will help to highlight literature clusters requiring further scrutiny.

3 Discussion

We developed a two-dimensional atlas of the biomedical literature based on the PubMed collection of 21 M paper abstracts using a transformer-based language model (PubMedBERT) and a neighbor embedding visualization (*t*-SNE) tailored to handle large document libraries. We used this atlas as an exploration tool to study the biomedical research landscape, generating hypotheses that we later confirmed using the original high-dimensional data. Using five distinct examples — the emergence of the Covid-19 literature, the evolution of the neuroscience discipline, the uptake of machine learning, the gender imbalance, and the concentration of retracted fraudulent pa-

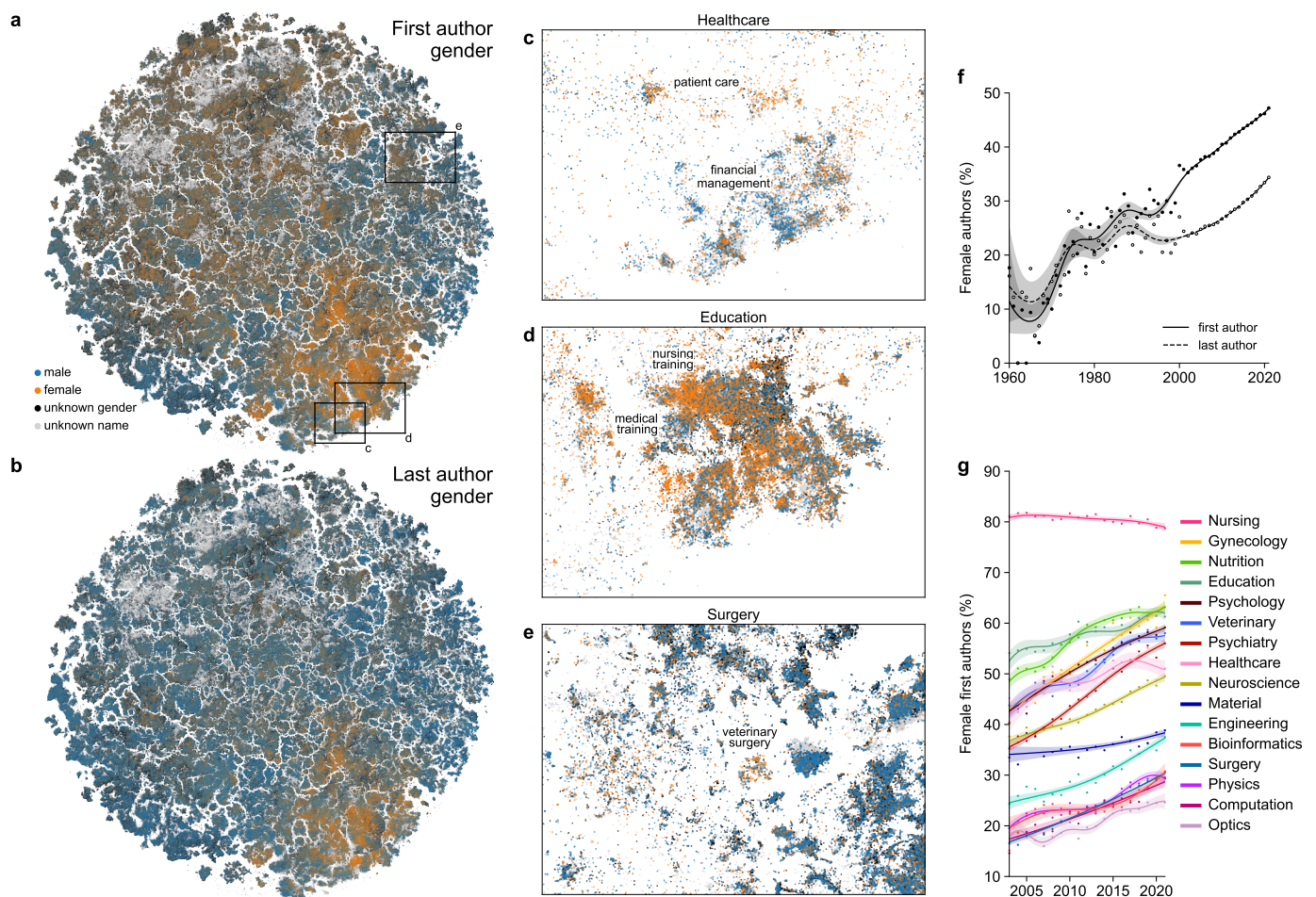


Figure 5: Gender bias in academic authorship. (a) Papers coloured by the inferred gender of their first authors. (b) Papers coloured by the inferred gender of their last authors. (c–e) Regions of the map showing within-label heterogeneity in the distribution of first authors' gender: in healthcare (c), education (d), and surgery (e). Only papers belonging to those labels are shown. (f) Fraction of female first and last authors across time. The amount of available first names increased dramatically after 2003 (Figure S1c). (g) Fraction of female first authors across time for different disciplines. Smooth curves and confidence intervals in panels (f,g) were obtained using generalized additive models (see Methods).

pers — we argued that two-dimensional visualizations of text corpora can help uncover aspects of the data that other analysis methods may fail to reveal.

We also developed an interactive web version of the embedding (<https://static.nomic.ai/pubmed.html>) based on the deepscatter library (Nomic AI, 2022) that allows to navigate the atlas, zoom, and search by title or journal name. In deepscatter, individual points are loaded on demand when zooming-in, like when navigating geographical maps in the browser.

Neighbor embedding methods like t-SNE have known limitations. For the datasets of our size, the few closest neighbors in the two-dimensional embedding space are typically different from the neighbors in the high-dimensional BERT representation (Table 1). This makes our map suboptimal for finding the most similar papers to a given query paper, and other tools, like conventional (Google Scholar, PubMed) or citation-based (connectedpapers.com) search engines, may be more appropriate for this task. Instead, our map is useful for navigating the literature on the scale of narrow and focused scientific topics. Neighbor embedding algorithms can misrepresent the global organization of the data (Wattenberg et al., 2016; Kobak and Berens, 2019; Böhm et al., 2022). We used methods designed to mitigate this issue (Kobak and Berens, 2019; Kobak and Linderman, 2021; González-Márquez et al., 2022), and indeed, found that related research areas were located close to each other.

Our atlas provides the most detailed visualization of the biomedical literature landscape to date. Previously, PubMed abstracts were clustered based on textual bag-of-words similarity and citation information, and the clusters were displayed using a two-dimensional embedding (Boyack et al., 2020). Their map exhibits similar large-scale organization, but only shows 29,000 clusters, so our map is almost three orders of magnitude more detailed. The BioBERT model was previously applied to the PubMed dataset to extract information on

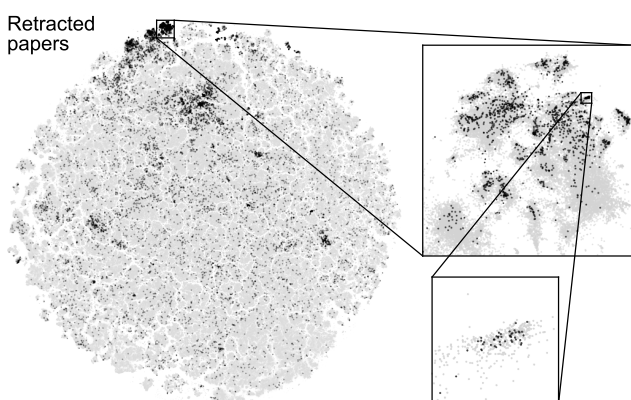


Figure 6: Retracted papers group together. All retracted papers with intact abstracts (11,756) are highlighted in black, plotted on top of the non-retracted papers. First inset corresponds to one of the regions with higher density of retracted papers (3.8%), covering research on cancer-related drugs, marker genes, and microRNA. Second inset corresponds to a subregion with a particularly high fraction of retracted papers (10.8%), the one we used for manual inspection.

biomedical concepts, such as proteins or drugs (Xu et al., 2020). Previous work on visualizing large text corpora includes Schmidt (2018) and González-Márquez et al. (2022). Both were based on bag-of-words representations of the data. Here we showed that BERT-based models outperform TF-IDF for representing scientific abstracts.

An alternative approach to visualizing collections of academic works is to use information on citations as a measure of similarity, as opposed to semantic or textual similarity. For example, paperscape.org visualizes 2.2 M papers from the *arXiv* preprint server using a force-directed layout of the citation graph. Similarly, opensyllabus.org uses node2vec (Grover and Leskovec, 2016) and UMAP to visualize 1.1 M texts based on their co-appearance in the US college syllabi. Similar approach was used by Noichl (2021) to visualize 68,000 articles on philosophy based on their reference lists. Here we based our embedding on the abstract texts alone, because citation information may not be easily available for all articles in the PubMed dataset. The functionality of our interactive web version is similar to opensyllabus.org and paperscape.org, but we successfully display one order of magnitude more points.

We achieved the best representation of the PubMed abstracts using the PubMedBERT model. As the progress in the field of language models is currently very fast, it is likely that a better representation may soon become available. One promising approach could be to train sentence-level models such as SBERT (Reimers and Gurevych, 2019) on the biomedical text corpus. Another active avenue of research is fine-tuning BERT models using contrastive learning (Gao et al., 2021; Liu et al., 2021) and/or using citation graphs (Cohan et al., 2020; Ostdorff et al., 2022). While we found that these models

were outperformed by PubMedBERT, similar methods (Yasunaga et al., 2022) could be used to fine-tune the PubMedBERT model itself, potentially improving its representation quality further. Finally, larger generative language models such as recently developed BioGPT (Luo et al., 2022) or BioMedLM (Stanford CRFM and MosaicML, 2022) can possibly lead to better representations as well.

In conclusion, we suggested a novel approach for visualizing large document libraries, and demonstrated that it can facilitate data exploration and help generate novel insights.

4 Methods

4.1 PubMed dataset

We downloaded the complete PubMed database (295 GB) as XML files using the bulk download service (www.nlm.nih.gov/databases/download/pubmed_medline.html). PubMed releases a new snapshot of their database every year; they call it a ‘baseline’. In our previous work (González-Márquez et al., 2022) we used the 2020 baseline (files called pubmed21n0001.xml.gz to 1062.xml.gz, download date: 26.01.2021). In this work, we supplemented them with the additional files from the 2021 baseline (files called pubmed22n1062.xml.gz to 1114.xml.gz, download date: 27.04.2022). After the analysis was completed, we realized that our dataset had 0.07% duplicate papers; they should not have had any noticeable influence on the reported results.

We used the Python `xml` package to extract PubMed ID, title, abstract, language, journal title, ISSN, publication date, and author names of all 33.4 M papers. We filtered out all 4.7 M non-English papers, 10.8 M papers with empty abstracts, 0.3 M papers with abstracts shorter than 250 or longer than 4000 symbols (Figures S1, S7), and 27 thousand papers with unfinished abstracts. Papers with unfinished abstracts needed to be excluded because otherwise they were grouped together in the BERT representation, creating artifact clusters in the embedding. We defined unfinished abstracts as abstracts not ending with a period, a question mark, or an exclamation mark. Some abstracts ended with a phrase “(ABSTRACT TRUNCATED AT ... WORDS)” with a specific number instead of ‘...’. We removed all such phrases and analyzed the remaining abstracts as usual, even though they did not contain the entire text of the original abstracts. This left 20,687,150 papers for further analysis.

This collection contains papers from the years 1808–2022. MEDLINE, the largest component of PubMed, started its record in 1966 and later included some noteworthy earlier papers. Therefore, the majority (99.8%) of the PubMed papers are post-1970 (Figure S1c). There are only few papers from 2022 in our dataset.

4.2 Label assignment

We labeled the dataset by selecting 38 keywords contained in journal titles that reflected the general topic of the paper. We based our choice of keywords on lists of medical specialties and life science branches that appeared frequently in the journal titles in our dataset. The 38 terms are: anesthesiology, biochemistry, bioinformatics, cancer, cardiology, chemistry, computation, dermatology, ecology, education, engineering, environment, ethics, genetics, gynecology, healthcare, immunology, infectious, material, microbiology, neurology, neuroscience, nursing, nutrition, ophthalmology, optics, pathology, pediatric, pharmacology, physics, physiology, psychiatry, psychology, radiology, rehabilitation, surgery, veterinary, and virology.

Papers were assigned a label if their journal title contained that term, either capitalized or not, and were left unlabeled otherwise. Journal titles containing more than one term were assigned randomly to one of them. This resulted in 7,123,706 labeled papers (34.4%).

Our journal-based labels do not constitute the ground truth for the topic of each paper, and so the highest possible classification accuracy is likely well below 100%. Nevertheless, we reasoned that the higher the classification accuracy, the better the embedding, and found this metric to be useful to compare different representations (Tables 1, 3).

4.3 BERT-based models

We used PubMedBERT (Gu et al., 2021) to obtain a numerical representation of each abstract. Specifically, we used the HuggingFace’s `transformers` library and the publicly released PubMedBERT model. PubMedBERT is a Transformer-based language model trained in 2020 on PubMed abstracts and full-text articles from PubMed Central.

In pilot experiments, we compared performance of eight BERT variants: the original BERT (Devlin et al., 2019), SciBERT (Beltagy et al., 2019), BioBERT (Lee et al., 2020), PubMedBERT (Gu et al., 2021), SBERT (Reimers and Gurevych, 2019), SPECTER (Cohan et al., 2020), SimCSE (Gao et al., 2021), and SciNCL (Ostendorff et al., 2022). The exact HuggingFace models that we used:

- bert-base-uncased
- allenai/scibert_scivocab_uncased
- dmis-lab/biobert-v1.1
- microsoft/BioMedNLP-PubMedBERT-base-uncased-abstract-fulltext
- sentence-transformers/all-mnlp-base-v2
- allenai/specter
- malteos/scincl
- princeton-nlp/unsup-simcse-bert-base-uncased

All of these models have the same architecture (`bert-base`; 110M parameters) but were trained and/or fine-tuned on different data. The original BERT was trained

Table 3: k NN accuracy of different BERT-based models. This comparison used a subset of the data (training set size: 990,000 labeled papers; test set size: 10,000 labeled papers). For comparison, the k NN accuracy values for the TF-IDF and SVD ($d = 300$) representations measured on the same subset were 61.0% and 54.8% respectively.

	Average	[CLS]	[SEP]
BERT	57.1%	50.4%	53.4%
SciBERT	62.1%	57.0%	60.9%
BioBERT	64.0%	62.7%	65.0%
PubMedBERT	64.4%	60.4%	67.7%
SBERT	64.5%	60.7%	62.2%
SPECTER	64.6%	63.9%	64.7%
SciNCL	65.9%	64.6%	64.6%
SimCSE	57.0%	53.2%	52.1%

on a corpus of books and text from Wikipedia. SciBERT was trained on a corpus of scientific articles from different disciplines. BioBERT fine-tuned the original BERT on PubMed abstracts and full-text articles from PubMed-Central. PubMedBERT was trained on the same data from scratch (and its vocabulary was constructed from PubMed data, whereas BioBERT used BERT’s vocabulary).

The other four models were fine-tuned to produce sentence embeddings instead of word embeddings, i.e. to generate a single vector representation of the entire input text (we treated each entire abstract as one single ‘sentence’ when providing it to these models). SBERT fine-tuned BERT using a corpus of similar sentences and paragraphs; the specific model that we used was obtained via fine-tuning MPNet (Song et al., 2020). According to SBERT’s authors, this is currently the most powerful generic SBERT model; note that their training procedure has evolved since the original approach described in Reimers and Gurevych (2019). SPECTER and SciNCL, both fine-tuned the SciBERT model using contrastive loss functions based on the citation graph. SimCSE fine-tuned the original BERT using a contrastive loss function between the sentence representations obtained with two different dropout patterns, using Wikipedia texts.

For this pilot experiment, we used a subset of our data ($n = 1,000,000$ labeled papers; 990,000 were used as a training set and 10,000 as a test set) to measure k NN accuracy ($k = 10$) of each of these models, and obtained the highest accuracy with PubMedBERT (see Table 3). This made sense as PubMedBERT’s training data largely overlapped with our dataset. We found that SBERT performed better than BERT, but did not reach the level of PubMedBERT on our task. SimCSE did not outperform the original BERT in our benchmark. SPECTER and SciNCL outperformed SciBERT, suggesting that citation information can be helpful for training scientific language models. Still, both models performed worse than PubMedBERT on our task.

Furthermore, we compared k NN accuracy after t -SNE

Table 4: k NN accuracy of t -SNE representations of different BERT-based models. The same experimental setup as in Table 3. For comparison, the accuracy of t -SNE of the TF-IDF representation (after SVD) was 49.9%.

	Average	[CLS]	[SEP]
BERT	46.0%	36.3%	40.6%
SciBERT	52.3%	43.4%	48.8%
BioBERT	54.7%	51.1%	56.5%
PubMedBERT	53.2%	45.5%	60.8%
SBERT	60.2%	56.3%	56.7%
SPECTER	58.4%	59.2%	59.3%
SciNCL	60.7%	59.1%	59.4%
SimCSE	46.9%	42.4%	40.3%

between different BERT models (Figure S8), and again obtained the best results with PubMedBERT (Table 4). The performance of SciNCL here was only 0.1% lower. We used the same settings for t -SNE as described below, but ran it with the default number of iterations (750).

Each abstract gets split into a sequence of tokens, and PubMedBERT represents each token in a 768-dimensional latent space. PubMedBERT’s maximum input length is 512 tokens and longer abstracts are automatically truncated at 512 tokens (this corresponds to roughly 300–400 words, and \sim 98% of all abstracts were shorter than 512 tokens). We are interested in a single 768-dimensional representation of each abstract, rather than 512 of them. For this, we compared several approaches commonly used in the literature: using the representation of the initial [CLS] token, the trailing [SEP] token, and averaging the representations of all tokens (Devlin et al., 2019; Reimers and Gurevych, 2019; Beltagy et al., 2019). Using the [SEP] token yielded the highest k NN accuracy in our pilot experiments (Table 3), so we adopted this approach.

Note that sentence transformers were originally trained to optimize one specific representation, e.g. SBERT uses the average representation across all tokens as its sentence-level output, while SPECTER uses the [CLS] token. For consistency, in Table 3 we report the performance of all three representations for each model. SBERT implementation (`sentence-transformers` library) normalizes its output to have norm 1. In Table 3 we report the accuracy without this normalization (64.5%), as obtained using the `transformers` library; with normalization, the accuracy changed by less than 0.1%.

Su et al. (2021) argued that whitening BERT representation can lead to a strongly improved performance on some benchmarks. We tried whitening the PubMedBERT representation, but only observed a decrease in the k NN accuracy. For this experiment, we used a test set of 500 labeled papers, and compared PubMedBERT without any transformations, after centering, and after whitening, using both Euclidean metric and the cosine metric, following Su et al. (2021). We obtained the best results using the raw PubMedBERT representation (Ta-

Table 5: k NN accuracy of label prediction using different transformations of the PubMedBERT representation and two different metrics for finding nearest neighbors. This experiment used test set size 500, smaller than in Table 1.

	Euclidean	Cosine
Raw	67.8%	67.8%
Centered	67.8%	67.4%
Whitened	64.2%	65.4%

ble 5). Our conclusion is that whitening does not improve the k NN graph of the PubMedBERT representation.

In the end, our entire collection of abstracts is represented as a $20,687,150 \times 768$ dense matrix.

4.4 TF-IDF representation

In our prior work (González-Márquez et al., 2022), we used the bag-of-words representation of PubMed abstracts and compared several different normalization approaches. We obtained the highest k NN accuracy using the TF-IDF (term frequency inverse document frequency) representation (Jones, 1972) with log-scaling, as defined in the scikit-learn implementation (version 0.24.1):

$$X_{ij} = (1 + \ln C_{ij}) \cdot \left(1 + \ln \frac{1 + n}{1 + \sum_k (C_{kj} > 0)} \right)$$

if $C_{ij} > 0$ and $X_{ij} = 0$ otherwise. Here n is the total number of abstracts and C_{ij} are word counts, i.e. the number of times word j occurs in abstract i .

The resulting dataset is a $20,687,150 \times 4,679,130$ sparse matrix (with 0.0023% non-zero elements), where 4,679,130 is the total number of unique words in all abstracts.

This matrix is too large to use in t -SNE directly, so for computational convenience we used truncated SVD (`sklearn.decomposition.TruncatedSVD` with `algorithm='arpack'`) to reduce dimensionality to 300, the largest dimensionality we could obtain given our RAM resources. Note that we did not use SVD when using the BERT representation and worked directly with the 768-dimensional representation.

4.5 t -SNE

We used the `openTSNE` (version 0.6.0) implementation (Poličar et al., 2019) of t -SNE (van der Maaten and Hinton, 2008) to reduce dimensionality from 768 (for the BERT representation) or 300 (for the TF-IDF representation) to $d = 2$. OpenTSNE is a Python reimplementation of the FIt-SNE (Linderman et al., 2019) algorithm.

We ran t -SNE following the procedure established in our prior work (González-Márquez et al., 2022): using uniform affinities (on the approximate k NN graph with $k = 10$) instead of perplexity-based affinities, early exaggeration annealing instead of the abrupt switch of the early exaggeration value, and extended optimization for

2250 iterations instead of the default 750 (250 iterations for the early exaggeration annealing, followed by 2000 iterations without exaggeration). We did not use any ‘late’ exaggeration after the early exaggeration phase. All other parameters were kept at default values, including PCA initialization and learning rate set to $n/12$, where n is the sample size. In our previous work we showed that this visualization approach outperformed UMAP (version 0.5.1) (McInnes et al., 2018) on PubMed data in TF-IDF representation in terms of both k NN recall and k NN accuracy (González-Márquez et al., 2022).

The t -SNE embeddings of a PubMed subset containing 1 million papers (Figure S8, Table 4) used the default number of iterations (750).

The embeddings based on the TF-IDF and PubMedBERT representation showed similar large-scale organization. As t -SNE loss function is unaffected by rotations and/or sign flips, we flipped the x and/or y coordinates of the TF-IDF t -SNE embedding to match its orientation to the PubMedBERT t -SNE embedding. The same was done for the embeddings shown in Figure S8.

4.6 Performance metrics

All k NN-based metrics were based on $k = 10$ exact nearest neighbors, obtained using the `NearestNeighbors` and `KNeighborsClassifier` classes from scikit-learn (version 1.0.2) using `algorithm='brute'` and `n_jobs=-1` (Pedregosa et al., 2011).

To predict each test paper’s label, k NN classifier takes the majority label among the paper’s nearest neighbors in the training set. To measure the accuracy, the classifier was trained on all labeled papers excluding a random test set of labeled papers. The test set size was 5000 for the high-dimensional representations and 10000 for the two-dimensional ones. The chance-level k NN accuracy was obtained using the `DummyClassifier` from scikit-learn with `strategy='stratified'`, and test set size 10000.

To predict each test paper’s publication year, we took the average publication year of the paper’s nearest neighbors in the training set. To measure the root-mean-squared error (RMSE), we used the training set consisting of all papers excluding a random test set. The test set size was 5000 for the high-dimensional representations and 10000 for the two-dimensional ones. The chance-level root-mean-squared error (RMSE) was calculated by drawing 10 random papers instead of nearest neighbors, for a test set of 5000 papers.

We define k NN recall as the average size of the overlap between k nearest neighbors in the high-dimensional space and k nearest neighbors in the low-dimensional space. We averaged the size of the overlap across a random set of 10000 papers for the BERT representation, and 5000 papers for the TF-IDF representation. The k NN recall value reported in Table 1 for the TF-IDF representation measures the recall of the original TF-IDF neighbors (0.7%); the recall of the neighbors from the SVD space (which was used for t -SNE) was 1.5%.

Isolatedness metric was defined as the average fraction of k nearest neighbors belonging to the same corpus. We used a random subset of 5000 papers from each corpus to estimate the isolatedness. The regions from Table 2 were selected as follows. The HIV/AIDS set contained all papers with ‘HIV’ or ‘AIDS’ words (upper case or lower case) appearing in the abstract. The influenza set contained all papers with the word ‘influenza’ in the abstract (capitalized or not). Similarly, meta-analysis set was obtained using the word ‘meta-analysis’. The virology and ophthalmology sets correspond to the journal-based labels (see above).

4.7 Covid-related papers

We considered a paper Covid-related if it contained at least one of the following terms in its abstract: ‘covid-19’, ‘COVID-19’, ‘Covid-19’, ‘CoViD-19’, ‘2019-nCoV’, ‘SARS-CoV-2’, ‘coronavirus disease 2019’, ‘Coronavirus disease 2019’. Our dataset included 132,802 Covid-related papers.

We selected 27 frequent terms contained in Covid-related paper titles to highlight different subregions of the Covid cluster. The terms were: antibody, anxiety, cancer, children, clinical, epidemic, healthcare, immune, implications, mental, mortality, outbreak, pediatric, pneumonia, population, psychological, respiratory, social, strategies, students, surgery, symptoms, therapy, transmission, treatment, vaccine, and workers. Papers were assigned a label if their title contained that term, either capitalized or not. Paper titles containing more than one term were assigned randomly to one of them. This resulted in 35,874 labeled Covid-related papers: 27.0% from the total amount of Covid-related papers and 45.6% of the Covid-related papers from the main Covid cluster in the embedding.

4.8 Generalized additive models

We used generalized additive models (GAMs) to obtain smooth trends for several of our analyses across time (Figures 3c, 4c, 5c–d). We used the `LinearGAM` (GAM with the Gaussian error distribution and the identity link function) and the `LogisticGAM` (GAM with the binomial error distribution and the logit link function) from the `pyGAM` Python library (version 0.8.0) (Servén and Brummitt, 2018). In all cases, we excluded papers published in 2022, since we only had very few of them (as we used the 2021 baseline of the PubMed dataset, see above). Linear GAMs (with `n_splines=6`) were used for Figure 3c, and logistic GAMs (with `n_splines=12`) were used for Figures 4c and 5c–d. All GAMs had the publication year as the only predictor.

In all cases, we used the `gridsearch()` function to estimate the optimal smoothing (`lambda`) parameter using cross-validation. To obtain the smooth curves shown in the plots, we predicted the dependent value on a grid of publication years. The confidence intervals were ob-

tained using the `confidenceintervals()` function from the same package.

In Figure 3c, the response variable was k NN overlap of a neuroscience paper with the target discipline. For each discipline, the input data was a set of 500 randomly chosen neuroscience papers for each year in 1975–2021. If the total number of neuroscience papers for a given year was less than 500, all of them were taken for the analysis. The k NN overlap values of individual papers were calculated using $k = 10$ nearest neighbors obtained with the `NearestNeighbors` class.

In Figure 4c, the binary response variable was whether a paper contained ‘machine learning’ in its abstract. For each discipline, the input data were all 2010–2021 papers.

In Figure 5c–d, the binary response variable was whether the paper’s first or last author was female (as inferred by the `gender` tool, see below). The input data in all cases were all papers with gender information from 1960–2021.

4.9 Gender prediction

We extracted authors’ first names from the XML tag `ForeName` that should in principle only contain the first name. However, we observed that sometimes it contained the full name. For that reason, we always took the first word of the `ForeName` tag contents (after replacing hyphens with spaces) as the author’s first name. This reduced some combined first names (such as Eva-Maria or Jose Maria) to their initial word (Eva; Jose). In many cases, mostly in older papers, the only available information about the first name was an initial. As it is not possible to infer gender from an initial, we discarded all extracted first names with length 1. In the end we obtained 13,429,169 first names of first authors (64.9% of all papers) and 13,189,271 first names of last authors (63.8%), almost only from 1960–2022.

We used the R package `gender` (Blevins and Mullen, 2015) (version 0.6.0) to infer authors’ genders. This package uses a historical approach that takes into account how naming practices have changed over time, e.g., Leslie used to be a male name in the early XX century but later has been mainly used as a female name. For each first/last author, we provided `gender` with the name and the publication year, and obtained the inferred gender together with a confidence measure.

The `gender` package offers predictions based on different training databases. We used the 1930–2012 Social Security Administration data from United States (`method='ssa'`). For the papers published before 1930 we fixed the year to 1930 and for the papers published after 2012, we fixed it to 2012. The SSA data do not contain information on names that are not common in the USA, and we only obtained inferred genders for 8,363,116 first authors (62.3% of available first names) and 8,468,165 last authors (63.1% of available last names). Out of all inferred genders, 3,543,592 first authors (42.4%) and 2,464,882 last authors (29.1%) were female.

Importantly, our gender inference is only approximate (Blevins and Mullen, 2015). The inference model has clear limitations, including limited US-based training data and state-imposed binary genders. Moreover, some first names are inherently gender-ambiguous. However, the distribution of inferred genders over biomedical fields and the pattern of changes over the last decades matched what is known about the gender imbalance in academia, suggesting that inferred genders were sufficiently accurate for our purposes.

4.10 Retracted papers

We obtained PMIDs of papers classified in PubMed as retracted (13,569) using PubMed web interface on 19.04.2023. Of those, 11,998 were present in our map (the rest were either filtered out in our pipeline or not included in the 2021 baseline dataset we used). To make sure that retracted papers were not grouping together in the BERT space because their abstract had been modified to indicate a retraction, we excluded from consideration all retracted papers containing the words “retracted”, “retraction”, “withdrawn”, or “withdrawal” in their abstract (242 papers). The remaining retracted papers (11,756) had intact original abstracts and are shown in Figure 6.

There was one small island at the bottom of the map containing retraction notices (they have independent PubMed entries with separate PMIDs) as well as corrigenda and errata, which were not filtered out by our length cutoffs. Many of the 242 retracted papers with post-retraction modified abstracts were also located there.

4.11 Runtimes

Computations were performed on a machine with 384 GB of RAM and Intel Xeon Gold 6226R processor (16 multi-threaded 2.90 GHz CPU cores) and on a machine with 512 GB of RAM and Intel Xeon E5-2630 v4 processor (10 multi-threaded 2.20 GHz CPU cores). BERT embeddings were calculated using an NVIDIA TITAN Xp GPU with 12.8 GB of RAM.

Parsing the XML files took 10 hours, computing the PubMedBERT embeddings took 74 hours, running t-SNE took 8 hours. More details are given in Table 6. We used exact nearest neighbors for all k NN-based quality metrics, so evaluation of the metrics took longer than computing the embedding. In total, it took around 8 days to compute all the reported metrics (Table 6).

Table 6: Runtimes for different analyses.

Step	Time
Parsing XML	10 h
PubMedBERT representation	74 h
TF-IDF representation	1 h
Truncated SVD of TF-IDF	4 h
<i>t</i> -SNE affinities for PubMedBERT	101 min
<i>t</i> -SNE affinities for TF-IDF	78 min
<i>t</i> -SNE optimization, 750 iter.	126 min
<i>t</i> -SNE optimization, 2250 iter.	390 min
<i>k</i> NNs for 1k papers, BERT	32 min
<i>k</i> NNs for 1k papers, BERT labeled	7 min
<i>k</i> NNs for 1k papers, TF-IDF	150 min
<i>k</i> NNs for 1k papers, TF-IDF labeled	12 min
<i>k</i> NNs for 1k papers, <i>t</i> -SNE	7 min
<i>k</i> NNs for 1k papers, <i>t</i> -SNE labeled	2 min
Table 1	~35 h
Table 2	~91 h
Figure 3c	~20 h
Table 3 (BERT computations)	~30 h
Table 4	~7 h
Table 5	~20 min
All GAMs	~30 min
Gender prediction	6 min

Data and code availability

The analysis code is available at <https://github.com/berenslab/pubmed-landscape>.

We made publicly available a processed version of our dataset: a `csv.zip` file (20,687,150 papers, 1.3 GB) including PMID, title, journal name, publication year, embedding x and y coordinates, our label, and our color used in Figure 1a. We also included two additional files: the raw abstracts (`csv.zip` file, 9.5 GB), and the 768-dimensional PubMedBERT embeddings of the abstracts (NumPy array in float16 precision, 31.8 GB). They can all be downloaded from <https://zenodo.org/record/7695389>.

Acknowledgments

We thank Richard Van Noorden, David Bimler, and Ivan Oransky for discussions. This research was funded by the Deutsche Forschungsgemeinschaft (KO6282/2-1, BE5601/8-1, and EXC 2064 “Machine Learning: New Perspectives for Science”, 390727645), by the German Ministry of Education and Research (Tübingen AI Center), and by the Hertie Foundation. The authors thank the International Max Planck Research School for Intelligent Systems (IMPRS-IS) for supporting Rita González Márquez.

Conflicts of Interest

Benjamin M. Schmidt is Vice President of Information at Nomic AI. The other authors declare no conflicts of interest.

References

- Iz Beltagy, Kyle Lo, and Arman Cohan. SciBERT: A pretrained language model for scientific text. In *Proceedings of the 2019 Conference on Empirical Methods in Natural Language Processing and the 9th International Joint Conference on Natural Language Processing (EMNLP-IJCNLP)*, pages 3615–3620, 2019.
- Michael HK Bendels, Ruth Müller, Doerthe Brueggemann, and David A Groneberg. Gender disparities in high-quality research revealed by nature index journals. *PLOS One*, 13(1):e0189136, 2018.
- Cameron Blevins and Lincoln Mullen. Jane, John... Leslie? A historical method for algorithmic gender prediction. *DHQ: Digital Humanities Quarterly*, 9(3), 2015.
- Jan Niklas Böhm, Philipp Berens, and Dmitry Kobak. Attraction-repulsion spectrum in neighbor embeddings. *Journal of Machine Learning Research*, 23(95):1–32, 2022.
- Katy Börner, Richard Klavans, Michael Patek, Angela M Zoss, Joseph R Biberstine, Robert P Light, Vincent Larivièvre, and Kevin W Boyack. Design and update of a classification system: The UCSD map of science. *PLOS One*, 7(7):e39464, 2012.
- Lutz Bornmann and Rüdiger Mutz. Growth rates of modern science: A bibliometric analysis based on the number of publications and cited references. *Journal of the Association for Information Science and Technology*, 66(11):2215–2222, 2015.
- Kevin W Boyack, Caleb Smith, and Richard Klavans. A detailed open access model of the PubMed literature. *Scientific Data*, 7(1):1–16, 2020.
- Jennifer Byrne. We need to talk about systematic fraud. *Nature*, 566(7742):9–10, 2019.
- Jennifer A Byrne and Jana Christopher. Digital magic, or the dark arts of the 21st century — how can journals and peer reviewers detect manuscripts and publications from paper mills? *FEBS Letters*, 594(4):583–589, 2020.
- Jennifer A Byrne and Cyril Labb  . Striking similarities between publications from China describing single gene knockdown experiments in human cancer cell lines. *Scientometrics*, 110(3):1471–1493, 2017.
- Jennifer A Byrne, Natalie Grima, Amanda Capes-Davis, and Cyril Labb  . The possibility of systematic research

- fraud targeting under-studied human genes: causes, consequences, and potential solutions. *Biomarker Insights*, 14:1177271919829162, 2019.
- Cristina Candal-Pedreira, Joseph S Ross, Alberto Ruano-Ravina, David S Egilman, Esteve Fernández, and Mónica Pérez-Ríos. Retracted papers originating from paper mills: cross sectional study. *BMJ*, 379, 2022.
- Arman Cohan, Sergey Feldman, Iz Beltagy, Doug Downey, and Daniel S Weld. Specter: Document-level representation learning using citation-informed transformers. In *Proceedings of the 58th Annual Meeting of the Association for Computational Linguistics*, pages 2270–2282, 2020.
- Jacob Devlin, Ming-Wei Chang, Kenton Lee, and Kristina Toutanova. BERT: Pre-training of deep bidirectional transformers for language understanding. In *Proceedings of NAACL-HLT*, pages 4171–4186, 2019.
- Jordan D Dworkin, Kristin A Linn, Erin G Teich, Perry Zurn, Russell T Shinohara, and Danielle S Bassett. The extent and drivers of gender imbalance in neuroscience reference lists. *Nature Neuroscience*, 23(8):918–926, 2020.
- Holly Else and Richard Van Noorden. The fight against fake-paper factories that churn out sham science. *Nature*, 591(7851):516–520, 2021.
- Giovanni Filardo, Brigit Da Graca, Danielle M Sass, Benjamin D Pollock, Emma B Smith, and Melissa Ashley-Marie Martinez. Trends and comparison of female first authorship in high impact medical journals: observational study (1994–2014). *BMJ*, 352, 2016.
- Tianyu Gao, Xingcheng Yao, and Danqi Chen. SimCSE: Simple contrastive learning of sentence embeddings. In *Proceedings of the 2021 Conference on Empirical Methods in Natural Language Processing*, pages 6894–6910, 2021.
- Rita González-Márquez, Philipp Berens, and Dmitry Kobak. Two-dimensional visualization of large document libraries using t-SNE. In *Proceedings of Topological, Algebraic, and Geometric Learning Workshops 2022*, volume 196 of *Proceedings of Machine Learning Research*, pages 133–141. PMLR, 25 Feb–22 Jul 2022.
- Aditya Grover and Jure Leskovec. node2vec: Scalable feature learning for networks. In *Proceedings of the 22nd ACM SIGKDD international conference on Knowledge discovery and data mining*, pages 855–864, 2016.
- Yu Gu, Robert Tinn, Hao Cheng, Michael Lucas, Naoto Usuyama, Xiaodong Liu, Tristan Naumann, Jianfeng Gao, and Hoifung Poon. Domain-specific language model pretraining for biomedical natural language processing. *ACM Transactions on Computing for Healthcare (HEALTH)*, 3(1):1–23, 2021.
- Karen Sparck Jones. A statistical interpretation of term specificity and its application in retrieval. *Journal of Documentation*, 1972.
- Dmitry Kobak and Philipp Berens. The art of using t-SNE for single-cell transcriptomics. *Nature Communications*, 10(1):1–14, 2019.
- Dmitry Kobak and George C Linderman. Initialization is critical for preserving global data structure in both t-SNE and UMAP. *Nature Biotechnology*, 39(2):156–157, 2021.
- Vincent Larivière, Chaoqun Ni, Yves Gingras, Blaise Cronin, and Cassidy R Sugimoto. Bibliometrics: Global gender disparities in science. *Nature*, 504(7479):211–213, 2013.
- Peder Larsen and Markus von Ins. The rate of growth in scientific publication and the decline in coverage provided by science citation index. *Scientometrics*, 84(3):575–603, 2010.
- Jinhyuk Lee, Wonjin Yoon, Sungdong Kim, Donghyeon Kim, Sunkyu Kim, Chan Ho So, and Jaewoo Kang. BioBERT: a pre-trained biomedical language representation model for biomedical text mining. *Bioinformatics*, 36(4):1234–1240, 2020.
- George C Linderman, Manas Rachh, Jeremy G Hoskins, Stefan Steinerberger, and Yuval Kluger. Fast interpolation-based t-SNE for improved visualization of single-cell RNA-seq data. *Nature Methods*, 16(3):243–245, 2019.
- Fangyu Liu, Ivan Vulić, Anna Korhonen, and Nigel Collier. Fast, effective, and self-supervised: Transforming masked language models into universal lexical and sentence encoders. In *Proceedings of the 2021 Conference on Empirical Methods in Natural Language Processing*, pages 1442–1459, 2021.
- Renqian Luo, Lai Sun, Yingce Xia, Tao Qin, Sheng Zhang, Hoifung Poon, and Tie-Yan Liu. BioGPT: generative pre-trained transformer for biomedical text generation and mining. *Briefings in Bioinformatics*, 23(6):bbac409, 2022.
- Leland McInnes, John Healy, and James Melville. UMAP: Uniform Manifold Approximation and Projection for dimension reduction. *arXiv preprint arXiv:1802.03426*, 2018.
- Maximilian Noichl. Modeling the structure of recent philosophy. *Synthese*, 198(6):5089–5100, 2021.
- Nomic AI. Deepscatter, 2022. URL <https://github.com/nomic-ai/deepscatter>.
- Malte Ostendorff, Nils Rethmeier, Isabelle Augenstein, Bela Gipp, and Georg Rehm. Neighborhood contrastive learning for scientific document representations with citation embeddings. *arXiv preprint arXiv:2202.06671*, 2022.

- F. Pedregosa, G. Varoquaux, A. Gramfort, V. Michel, B. Thirion, O. Grisel, M. Blondel, P. Prettenhofer, R. Weiss, V. Dubourg, J. Vanderplas, A. Passos, D. Cournapeau, M. Brucher, M. Perrot, and E. Duchesnay. Scikit-learn: Machine learning in Python. *Journal of Machine Learning Research*, 12:2825–2830, 2011.
- Pavlin G Poličar, Martin Stražar, and Blaž Zupan. openTSNE: a modular Python library for t-SNE dimensionality reduction and embedding. *BioRxiv*, page 731877, 2019.
- Nils Reimers and Iryna Gurevych. Sentence-BERT: Sentence embeddings using siamese BERT-networks. In *Proceedings of the 2019 Conference on Empirical Methods in Natural Language Processing and the 9th International Joint Conference on Natural Language Processing (EMNLP-IJCNLP)*, pages 3982–3992, 2019.
- Benjamin Schmidt. Stable random projection: Lightweight, general-purpose dimensionality reduction for digitized libraries. *Journal of Cultural Analytics*, 2018.
- Daniel Servén and Charlie Brummitt. pyGAM: Generalized additive models in python, 2018. URL <https://doi.org/10.5281/zenodo.1208723>.
- Yiqin Alicia Shen, Jason M Webster, Yuichi Shoda, and Ione Fine. Persistent underrepresentation of women’s science in high profile journals. *BioRxiv*, page 275362, 2018.
- Kaitao Song, Xu Tan, Tao Qin, Jianfeng Lu, and Tie-Yan Liu. Mpnet: Masked and permuted pre-training for language understanding. *Advances in Neural Information Processing Systems*, 33:16857–16867, 2020.
- Stanford CRFM and MosaicML. BioMedLM, 2022. URL <https://huggingface.co/stanford-crfm/BioMedLM>.
- Jianlin Su, Jiarun Cao, Weijie Liu, and Yangyiwen Ou. Whitening sentence representations for better semantics and faster retrieval. *arXiv preprint arXiv:2103.15316*, 2021.
- Laurens van der Maaten and Geoffrey Hinton. Visualizing data using t-SNE. *Journal of Machine Learning Research*, 9(11), 2008.
- Ashish Vaswani, Noam Shazeer, Niki Parmar, Jakob Uszkoreit, Llion Jones, Aidan N Gomez, Łukasz Kaiser, and Illia Polosukhin. Attention is all you need. *Advances in Neural Information Processing Systems*, 30, 2017.
- Martin Wattenberg, Fernanda Viégas, and Ian Johnson. How to use t-SNE effectively. *Distill*, 1(10):e2, 2016.
- Jian Xu, Sunkyu Kim, Min Song, Minbyul Jeong, Donghyeon Kim, Jaewoo Kang, Justin F Rousseau, Xin Li, Weijia Xu, Vette I Torvik, et al. Building a PubMed knowledge graph. *Scientific Data*, 7(1):1–15, 2020.
- Michihiro Yasunaga, Jure Leskovec, and Percy Liang. LinkBERT: Pretraining language models with document links. In *Association for Computational Linguistics (ACL)*, 2022.
- Tianye Zhao, Tiancong Dai, Zhijun Lun, and Yanli Gao. An analysis of recently retracted articles by authors affiliated with hospitals in mainland China. *Journal of Scholarly Publishing*, 52(2):107–122, 2021.

A Appendix

A.1 Supplementary Tables

Table S1: Percentage of abstracts mentioning various machine learning methods (as in Figure 4a) in each region of the embedding with high fraction of abstracts mentioning ‘machine learning’ (Figure 4b). Percentages above 4% in bold. Rows ordered by the number of papers in the region. Columns ordered by the average percentage across regions. Abbreviations as in Figure 4.

#	Region	NN	Clustering	DL	SVM	CNN	PCA	RF	LR	DR	FA
1	EEG signals	6.1	1.7	1.9	3.3	2.1	1.1	0.8	0.8	0.4	0.2
2	Sequencing	1.5	5.8	1.0	0.9	0.7	0.4	0.6	0.3	0.3	0.1
3	Image segmentation	9.5	2.4	7.3	2.5	7.6	0.9	1.0	0.5	0.2	0.1
4	ML algorithms	14.7	5.7	4.3	2.9	5.1	1.1	0.6	0.5	0.9	0.2
5	Mass spectrometry	1.8	1.2	0.2	1.5	0.2	4.9	0.4	1.1	0.2	0.5
6	Healthcare data	1.7	0.8	1.6	0.6	0.6	0.0	0.2	0.0	0.0	0.0
7	Cancer biomarkers	0.5	4.9	0.2	1.0	0.1	1.1	0.8	0.3	0.1	0.1
8	Protein structure	5.5	3.5	1.9	4.6	1.0	0.7	1.7	1.4	0.3	0.1
9	Computational chemistry	1.9	0.4	0.3	0.1	0.2	0.1	0.1	0.2	0.1	0.0
10	Tumor imaging	3.3	1.2	2.8	3.6	2.0	0.7	2.6	1.3	0.3	0.1
11	Microbiome	0.1	2.9	0.0	0.2	0.0	1.2	1.5	0.9	0.0	0.1
12	Covid-19 tweets	1.5	2.1	1.9	0.7	0.4	0.2	0.8	0.6	0.0	0.0

A.2 Supplementary Figures

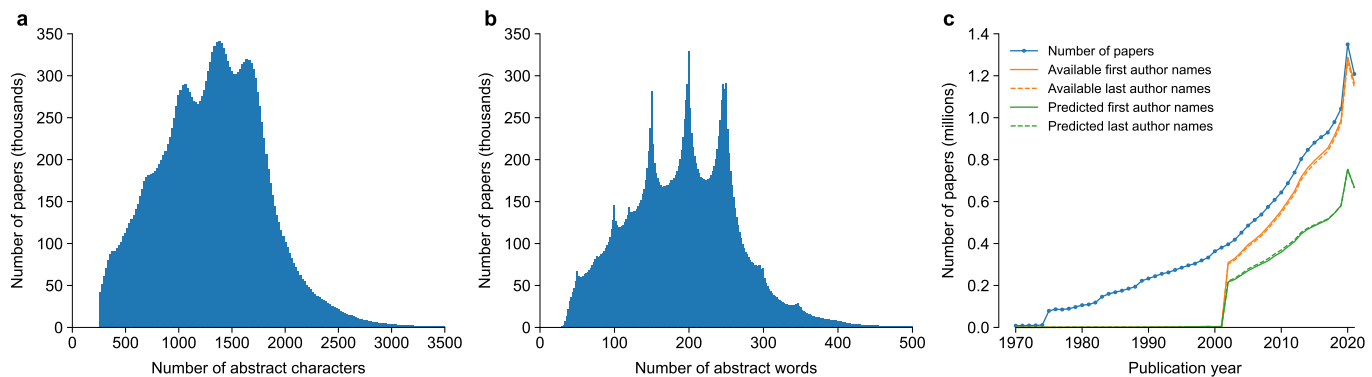


Figure S1: Summary of the PubMed dataset. (a) Distribution of the abstract length in characters. For the distribution of the abstract length over the embedding, see Figure S7. Papers with abstracts shorter than 250 characters were filtered out (see Methods). (b) Distribution of the abstract length in words. (c) The total number of papers per year, the number of available first/last authors’ first names per year, and the number of inferred first/last author genders per year. The amount of available first names increased dramatically after 2003, when PubMed began incorporating more detailed author information into their database (97.4% of available first names are post-2003).

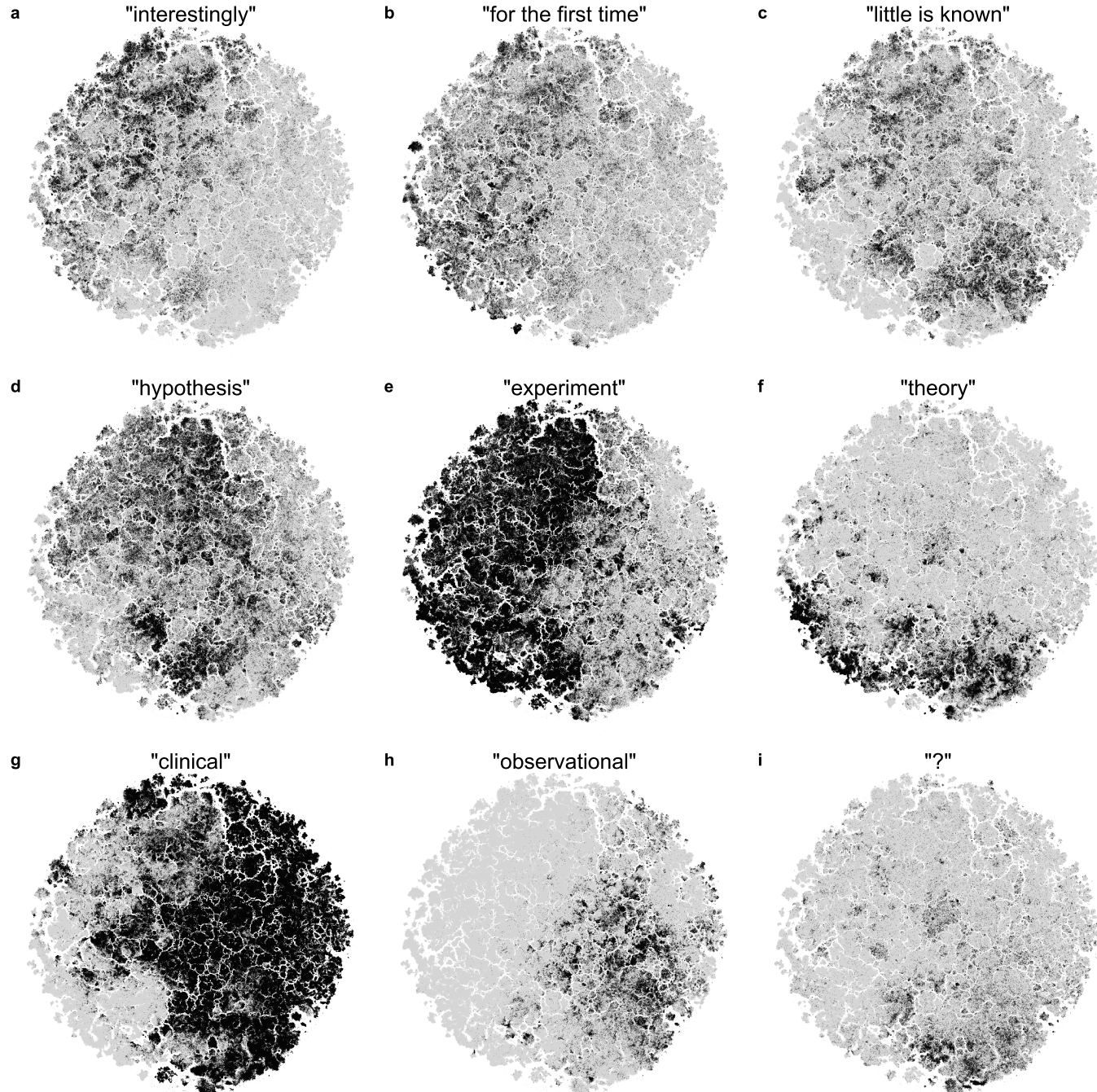


Figure S2: Distribution of some terms and phrases across the biomedical literature. All panels show the embedding based on the PubMedBERT representation, highlighting papers containing particular terms in their abstracts. (a) ‘interestingly’, (b) ‘for the first time’. Two black islands stand out in the periphery of the embedding: the one in the bottom contains articles reporting new species (‘species nova’) and the one on the left contains articles reporting novel chemical compounds isolated from living organisms. (c) ‘little is known’, (d) ‘hypothesis’, (e) ‘experiment’, (f) ‘theory’, (g) ‘clinical’, (h) ‘observational’, (i) ‘?’ (question mark).

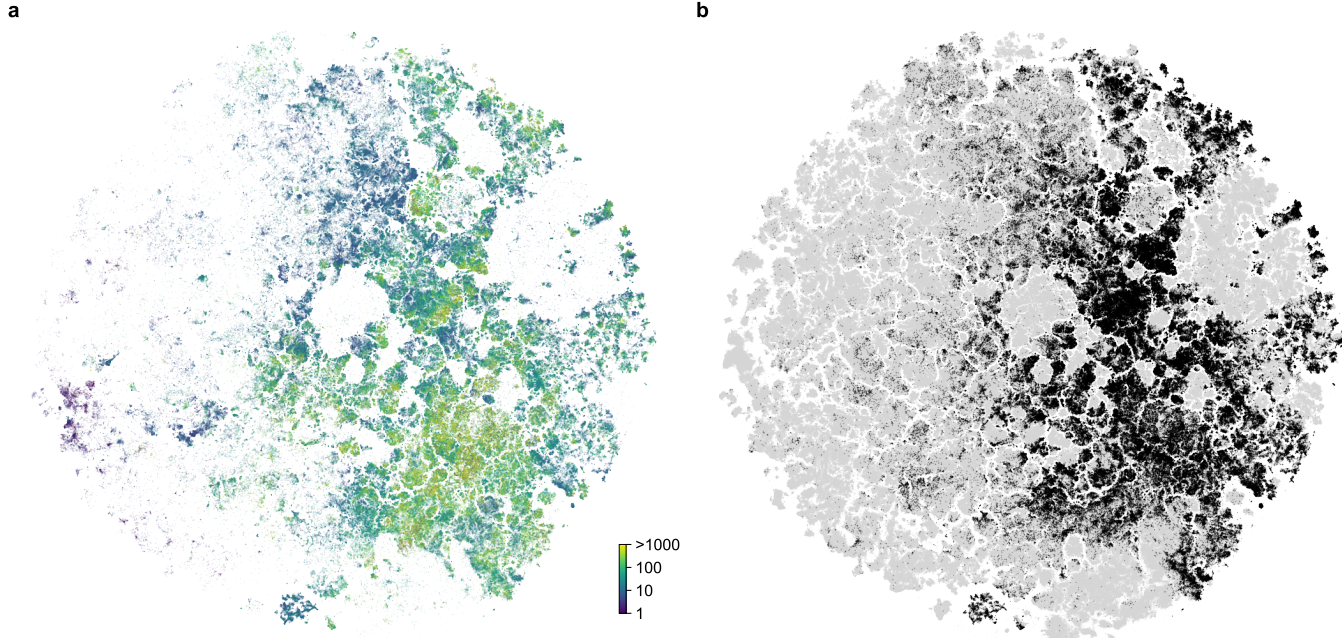


Figure S3: Distribution of reported sample sizes and p -values across the biomedical landscape. (a) Embedding coloured by the sample size reported in the abstract. We used the regular expression `n\s?=\s?(\d+)` to extract the reported sample sizes. If an abstract contained several reported sample sizes, we took the first one. Color scale on the log scale, dark: $n = 1$; light: $n \geq 1000$. Papers that did not contain this regular expression in their abstracts are not displayed. (b) Papers reporting p -values in their abstracts (containing ‘ $p=$ ’ or ‘ $p<$ ’ strings, with or without space after ‘ p ’) are shown in black.

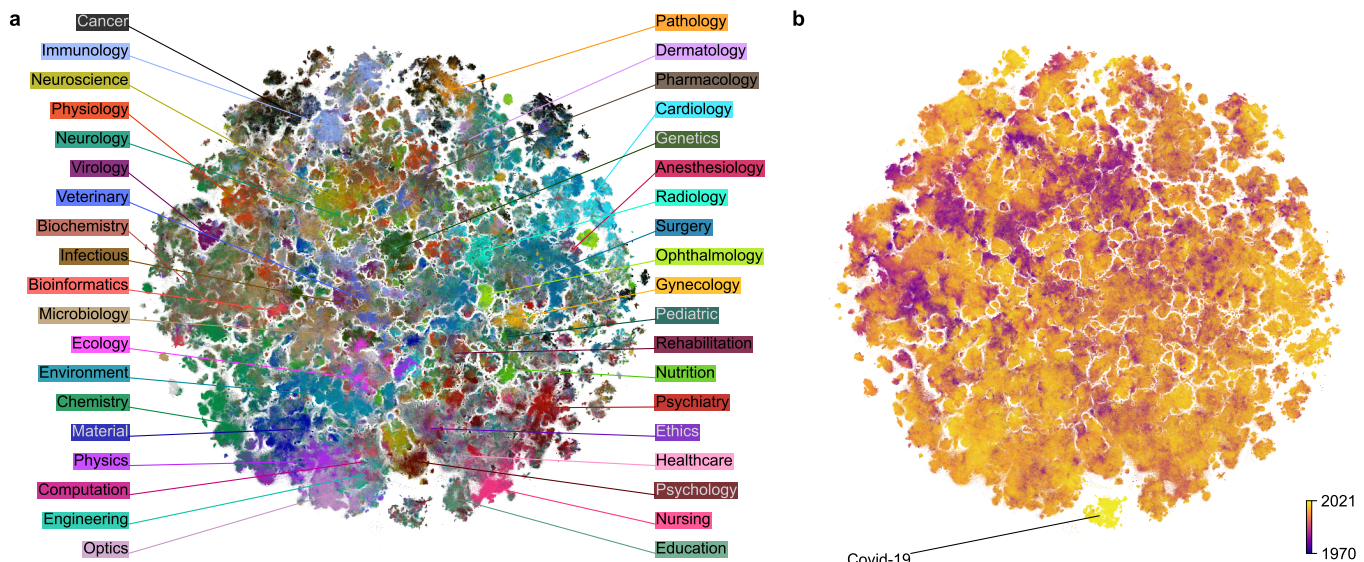
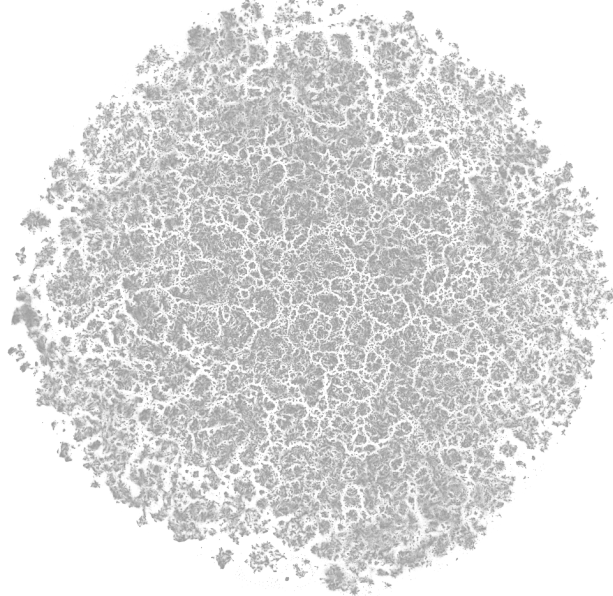


Figure S4: 2D embedding based on the TF-IDF representation of the PubMed dataset. (a) Coloured using labels based on journal titles. Unlabeled papers are shown in gray and are displayed in the background. The TF-IDF-based embedding was flipped to orient it similarly to the BERT-based embedding (Figure 1). (b) Coloured by publication year (dark: 1970 and earlier; light: 2021).

a BERT



b TF-IDF

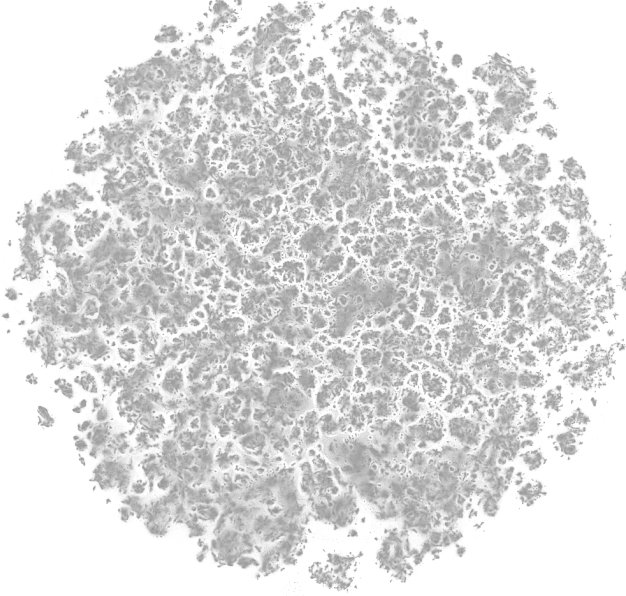
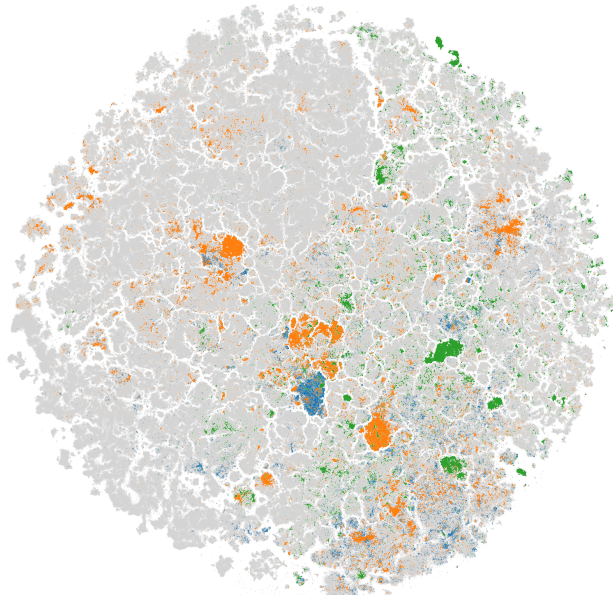


Figure S5: Fine cluster structure in the PubMed embeddings. All points shown in gray to emphasize the cluster structure. (a) The embedding based on the PubMedBERT representation. (b) The embedding based on the TF-IDF representation.

a BERT



b TF-IDF

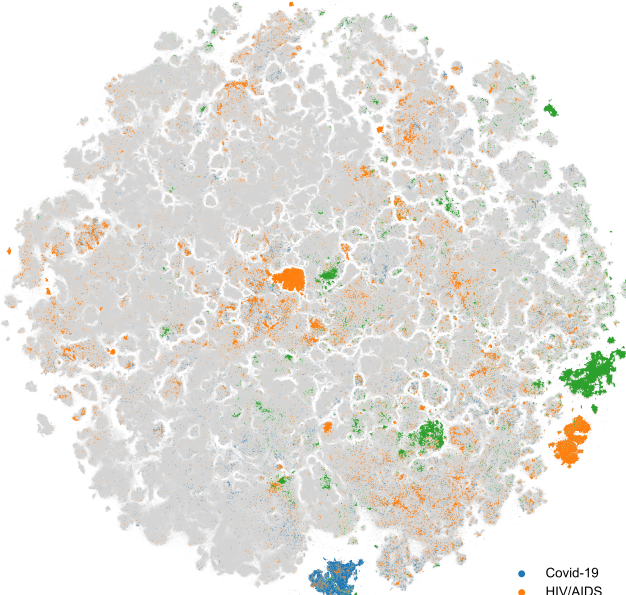
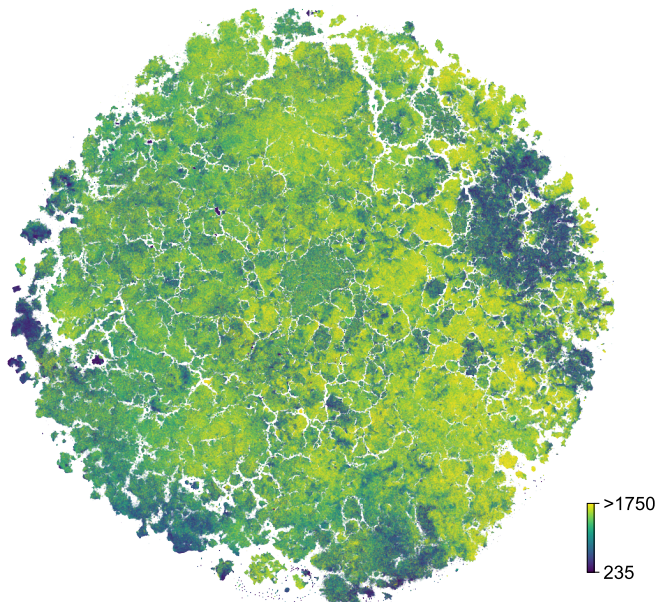


Figure S6: Isolated subcorpora in the PubMed embeddings. Three sets of papers analyzed in Table 2 (Covid-19, HIV/AIDS, meta-analysis) highlighted in both embeddings. (a) PubMedBERT-based embedding. (b) TF-IDF-based embedding.

a Abstract length



b Title length

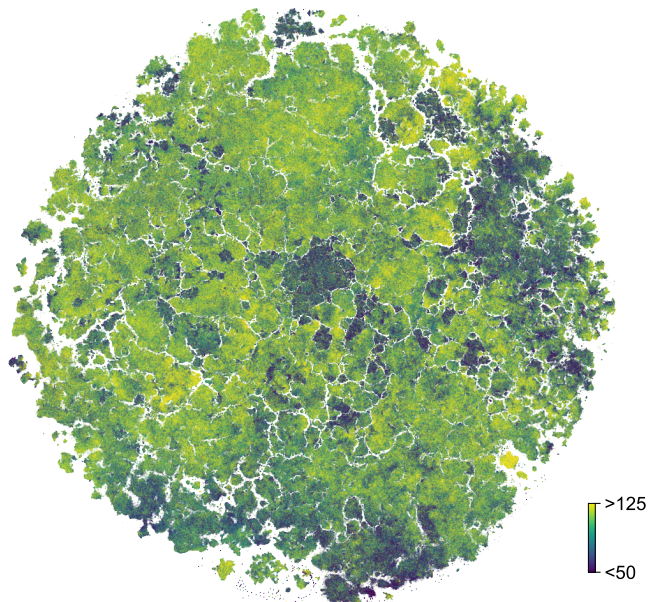


Figure S7: Distribution of abstract and title lengths across the biomedical literature. Both panels show the embedding based on the PubMedBERT representation of the PubMed dataset. (a) Coloured by the length of the abstract (dark: 235 characters; light: 1750 characters or more). (b) Coloured by the length of the title (dark: 50 characters or less; light: 125 characters or more).

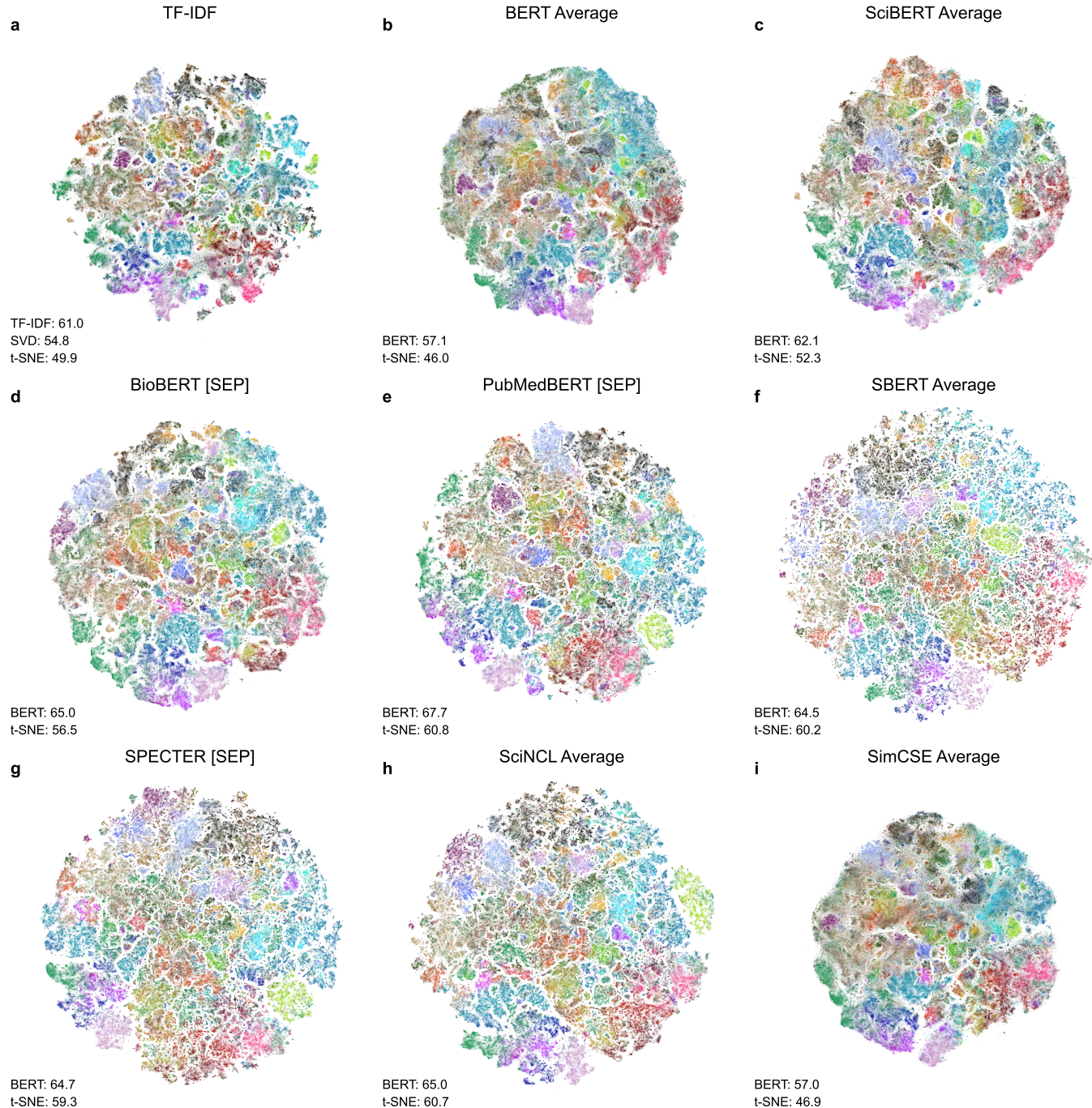


Figure S8: t-SNE embeddings of a subset of the PubMed dataset based on different representations. Subset size: 1,000,000 labeled papers. For each BERT-based model, we chose the two-dimensional embedding based on the representation (average, [CLS], or [SEP] token) with the highest kNN accuracy, see Table 4. The kNN accuracies for the high-dimensional and two-dimensional representations are shown in the corner of each panel. The embeddings were flipped to orient them similarly to the embedding of the full dataset (Figure 1). (a) TF-IDF (using SVD), (b) BERT, (c) SciBERT, (d) BioBERT, (e) PubMedBERT, (f) SBERT, (g) SPECTER, (h) SciNCL, (i) SimCSE.